Boosting L-type Ca^{2+} channel activity in tuberous sclerosis mitigates excess glutamate receptors and seizures

Farr Niere[1†], Luisa P. Cacheaux[,1†], David C. Klorig[2], William C. Taylor[1], Thuy Smith[2], Dwayne W. Godwin[1,2], and Kimberly F. Raab-Graham[1*]

Affiliations: [1]Department of Physiology and Pharmacology, [2]Department of Neurobiology and Anatomy, Wake Forest School of Medicine, Medical Center Boulevard, Winston-Salem, NC 27157, USA.

[†]Equal contribution

* To whom correspondence should be addressed: Kimberly F. Raab-Graham, Ph.D. Department of Physiology and Pharmacology, Wake Forest University Health Sciences, Medical Center Boulevard, Winston-Salem, NC 27157-1083

E-mail: kraabgra@wakehealth.edu

Abstract

Tuberous sclerosis complex (TS) is a dominant, multisystem disorder with devastating neurological symptoms. Approximately 85% of TS patients suffer from epilepsy over their lifespan and roughly 25-50% of those patients develop Autism Spectrum Disorder (1, 2). Current seizure therapies are effective in some, but not all, and often have significant risk factors associated with their use (1, 3). Thus, there is a critical need for new medication development or drug repositioning. Herein, we leveraged proteomic signatures of epilepsy and ASD, often comorbid in TS, to utilize an *in silco* approach to identify new drug therapies for TS-related seizures. We have discovered that activation of L-type voltage dependent calcium channels (L-VDCC) by Bay-K8644 (BayK) in a preclinical mouse model of TS curtails seizure frequency. Remarkably, at the molecular level, excess expression of ionotropic, AMPA-subtype glutamate (GluA) receptors is rescued by the administration of BayK. As added proof of BayK working through L-VDCC to regulate GluA levels, we found that increasing expression of alpha2delta2 (α2δ2), an auxiliary calcium channel subunit that boosts L-VDCC surface expression, similarly lowers the surface expression of dendritic GluA in TS. These BayK-induced molecular and functional alterations may underlie the longer lifespan of TS mice treated with BayK.

Keywords

alpha2delta2 (α2δ2); autism spectrum disorder; Cacna2d2; calcium channels; connectivity mapping; disease-disease interaction; DJ-1; drug repurposing; epilepsy; glutamate receptors; mammalian target of rapamycin (mTOR); mRNA; Parkinsonism

associated deglycase; Parkinson disease (autosomal recessive, early onset) 7; postsynaptic density; protein homeostasis; RNA-binding protein; synapses; tuberous sclerosis complex

Significance Statement

Causal mechanisms of Tuberous Sclerosis (TS)-associated neurological disorders are under-characterized and treatment options are lacking. Using a computational approach of mTOR/DJ-1 target mRNAs to predict new medications, we report that boosting L-type voltage-dependent Ca^{2+} channel (L-VDCC) activity in a preclinical TS mouse model that exhibits a deficit in dendritic L-VDCC activity ameliorates key molecular and electrophysiological pathologies that are predicted to underlie seizures. Additionally, boosting L-VDCC activity extends lifespan. Restoring the mTOR/DJ-1 pathway upstream of L-VDCC, therefore, may serve as a new therapeutic avenue to mitigate seizures and mortality in TS.

Introduction

The majority of patients with TS struggle with neurological and neuropsychiatric problems throughout their lifetime (4). The etiology of TS stems from loss-of-function mutations of either the *TSC1* or *TSC2* gene. Normally, Tsc1 and Tsc2 proteins work in conjunction to limit the activity of the mammalian target of rapamycin complex 1 (mTORC1), a key signaling pathway in protein homeostasis (5). Numerous investigations on mTORC1 demonstrate that its activity can equally promote and inhibit protein expression, especially in synaptic regions (6-10). Emerging studies now also indicate that persistent over- or underactive mTORC1 state can steer neuronal and network excitability towards pathological conditions, as mTORC1 regulates the expression of ion channels and their associated proteins (7, 11-13) *(see accompanying manuscript)*. Indeed, several diseases—epilepsy and autism spectrum disorder (ASD) to name a few—that exhibit persistent mTORC1 activity also have enduring states of neuronal or network hyperexcitability (14-17). A mechanism by which mTORC1 can influence ion channel expression and activity, and potentially behavior, is by controlling the levels of RNA-binding proteins (RBPs). RBPs profoundly impact the translation and/or stability of target mRNAs (5, 9, 18) *(see accompanying manuscript)*. By regulating the expression or repression of their target mRNAs, RBPs have the capacity to coordinate the synaptic function (5, 19). We have recently discovered that mTORC1 can dampen dendritic L-type voltage-dependent calcium (Ca^{2+}) channel (L-VDCC) activity through the RNA-binding protein DJ-1 (encoded by *Park7*) *(see accompanying manuscript)*. In a preclinical, mouse model of TS, in which *Tsc1* has been conditionally knocked-out (*Tsc1* KO), DJ-1 expression is elevated in dendrites and postsynaptic

density (PSD)-positive regions (9). In light of the changes in DJ-1's subcellular localization in response to mTORC1 activity and DJ-1's ability to control protein expression of its target mRNAs, we explored the therapeutic potential of mitigating DJ-1/L-VDCC signaling in TS.

Results

Prediction of Bay-K-8644 to oppose the effects of aberrant mTOR/DJ-1 at the synapse

As a first step in evaluating if DJ-1 plays a relevant role in TS and the PSD, we searched the mRNA transcripts that encode PSD-associated proteins for DJ-1 binding sites (9) *(see accompanying manuscript)* (**Table S1**). Remarkably, ~13% of risk genes for TS-associated neurological disorders (epilepsy and autism spectrum disorder (ASD)) are PSD-associated proteins that are encoded by mRNAs possessing DJ-1-binding motifs (**Fig. 1A; Tables S2 and S3**). With putative DJ-1-target mRNAs in hand, we used an unbiased, bioinformatics approach to pinpoint specific DJ-1 function and to identify potential new therapeutic reagents. To accomplish this, we used connectivity mapping (CMap)—an algorithm that can be used to predict drugs that may match or oppose a given change in a gene-expression profile (20). We hypothesized that DJ-1-target mRNAs—predicted to be repressed when mTORC1 is overactive—are homeostatic and neuroprotective. Inputting putative DJ-1-target mRNAs that are predicted to go up when mTOR is off, surprisingly identified Bay-K-8644 (BayK)—an L-VDCC opener—as a candidate-drug with a score of 97 (**Table S4**). A tau score that is higher than 90 is generally considered a compelling candidate for further study (21). Also in line with our hypothesis, L-VDCC is thought to mediate homeostasis (22).

CMap analysis suggests that treating TS with BayK will reverse DJ-1 expression—returning it back to WT levels—and restore L-VDCC-mediated functions despite the significant deficit in dendritic L-type activity *(see accompanying manuscript)*. To test this prediction, we generated a preclinical mouse model of TS, whereby *Tsc1* was conditionally knocked out (*Tsc1* KO) in *Tsc1*^{tm1Djk}*/J* mice by stereotaxically introducing AAV-Cre-GFP or AAV-GFP, which serves as control, in the hippocampi. mTORC1 activity and DJ-1 levels in dendrites and PSD-positive regions are elevated in TS mice—those that received Cre-GFP—compared to controls (9). We then gave TS mice a single injection of BayK (0.2-2mg/kg) intraperitoneally (i.p.) and measured synaptic DJ-1 protein levels 18-20 hours post-injection. Results of western blot assays indeed indicate that BayK treatment can restore DJ-1 protein levels in TS synaptoneurosomes down to WT level, as predicted by CMap analyses (**Fig. 1B**).

BayK restores elevated membrane-surface GluA in TS to wildtype condition

L-VDCC performs many cellular functions, including promoting endocytosis of AMPA-subtype glutamate receptors (GluA) (23). It's been reported that GluA1 levels are elevated in the human condition of TS (24). Moreover, GluA-mediated currents are enhanced in a *Tsc1* KO mouse model (25, 26). To mimic L-VDCC hypofunction in TS and to assess the impact of reduced L-type channel activity on GluA expression, we blocked L-type activity of dissociated WT hippocampal neurons with 5 μM nimodipine for 30 minutes and subsequently measured the surface expression of GluA (sGluA) on dendrites by immunocytochemistry. Of note, sGluA levels correlate well with GluA-mediated currents (27-29). L-VDCC blockade by nimodipine increases sGluA by

~twofold over control (**Fig. 2A and B**). Building on this result, we treated dissociated hippocampal neurons from TS mice with 5 μM BayK for 60 minutes and assessed sGluA expression. Our results show that TS neurons, compared to WT, express twofold more sGluA. Furthermore, applying BayK to TS neurons lowers their sGluA levels to WT state (**Fig. 2C and D**).

Overexpression of DJ-1-repressed α2δ2 restores elevated membrane-surface GluA in TS to WT condition

Since DJ-1 lowers the dendritic level of α2δ2, which facilitates the surface membrane expression of pore forming Ca^{2+} channel subunits and increases current density, we investigated the influence of α2δ2 on sGluA expression (30-32). TS dendrites notably have more GluA but less α2δ2 than WT *(see accompanying manuscript)*. We therefore considered the possibility that overexpressing α2δ2 in dissociated rat neurons would curtail sGluA expression. Overexpressing *Cacna2d2*—the gene that encodes α2δ2 protein—as predicted lowers sGluA expression (**Fig. 2E and F**). Additionally, increasing α2δ2 levels in TS restores sGluA to WT level (**Fig. 2G and H**). These findings collectively demonstrate that DJ-1 can modulate postsynaptic function through L-VDCC.

In vivo administration of BayK ameliorates the exaggerated protein expression of GluA and ribosomal S6 in TS

As our *in vitro* data indicate that BayK can mitigate the overabundance of GluA in TS, we assessed BayK's effect *in vivo*. TS mice were treated with vehicle or the same

concentration of BayK that lowers DJ-1 expression to WT level (**Fig. 1B**). Eighteen to twenty hours post-injection, we measured a population of GluA that is phosphorylated at serine 845 residue (pGluA1), which is associated with increased GluA-mediated synaptic current (33). By western blot assays of hippocampal synaptoneurosomes, pGluA1 expression in BayK-treated mice showed a direction towards WT condition, although it did not reach significance (**Fig. 3A and B**). Total GluA expression, however, showed a marked reduction in BayK-injected TS mice compared to vehicle-treated (**Fig. 3C**). Because increases in GluA expression is sensitive to mTOR activity, we examined whether BayK can dampen mTOR activity by measuring the levels of phospho-S6 (pS6)—a downstream effector of mTOR activity—in vehicle and BayK-treated TS animals (34, 35). BayK does reduce pS6 expression in TS; but, BayK does not lower pS6 to WT levels (**Fig. 3D and E**). BayK, however, curtails total S6 to WT condition (**Fig. 3F**). These data suggest that BayK possesses a therapeutic value in TS, as a single peripheral administration of BayK can correct GluA expression by partially repressing mTORC1 activity.

BayK mitigates electrogenic seizures in TS

The majority of humans with TS experience seizures in their lifetime (36-38). Of note, humans with epilepsy have an overabundance of GluA (39). Since BayK lowers GluA levels, we hypothesized that boosting L-VDCC activity will attenuate seizures. To do this, we recorded local field potentials using a chronic recording array implanted in hippocampal CA1 of freely behaving *Tsc1* KO mice (9, 40). Approximately three weeks after introducing AAV-Cre-GFP and implanting the electrodes, TS mice received a

single i.p. injection of vehicle or BayK (0.2-1.0 mg/kg) and subsequently were monitored for electrophysiological seizures. We assessed the efficacy of BayK on the severity of seizures by measuring the frequency and duration of seizures throughout the lifespan of each animal (**Fig. 3G**). All three vehicle-treated animals developed seizures electrophysiologically; however, only one out of the three BayK-treated animals had seizures. Because a single administration of BayK shows a trend towards a reduction in seizure events, we hypothesized that chronic administration of BayK (every 6 days) would further reduce the electrophysiological seizures in TS. Similar to acutely treated subjects, TS mice that received chronic BayK treatment have fewer seizures. However, unlike the acute administration, all animals that received chronic injections manifest seizures. Since there is no significant difference between single- and multiple-injected subjects, we combined the data of these two groups. BayK treatment robustly mitigates electrogenic seizures in TS. Compared to the vehicle treatment BayK lowers the frequency of seizures by fivefold and the duration of seizures by sevenfold group, the frequency of seizures in BayK-treated is three-fold less and the duration of seizures (**Fig. 3H and I**). These findings altogether suggest that peripheral administration of BayK may be a suitable treatment to mitigate seizures in TS.

BayK extends lifespan of TS

TS-associated disruptions in the brain lowers life expectancy in humans (41-43). Seizures, of note, are a risk factor for mortality (43, 44). Because BayK lowers the frequency and duration of seizures, we examined if an acute i.p. injection of BayK can extend lifespan. Exposed to similar physical stressors (e.g. handling and recordings),

the lifespan of chronically implanted TS animals is significantly reduced relative to chronically implanted GFP/control (WT) mice, consistent with the human literature (**Fig. 4A**) (38, 41-43, 45). Importantly, TS mice—implanted for recording and non-implanted—that received a single treatment of BayK live ~27% longer than their respective vehicle-treated group **(Fig. 4B**).

Discussion

The symptoms of TS include epilepsy, ASD and intellectual disability (1, 46-48). As these symptoms implicate postsynaptic dysfunctions, our PSD-targeted, bioinformatics approach using CMap reveals that activating L-type VDCC may mitigate TS-associated neurological disorders (**Fig. 1**). This finding is indeed surprising as L-type channel agonists are rarely considered as therapeutic. Administered to normal organisms, L-VDCC activation can induce neurological and neuropsychiatric symptoms (49). In TS where L-type channel activity is low at best, agonism of the channel is beneficial as it can reduce excess GluA receptors from the membrane surface (**Fig. 2**). Moreover, L-type activation by BayK curtails seizure frequency in a preclinical model of TS (**Fig 3**). As a consequence of fewer seizures, BayK treatment may improve the quality of life and reduce mortality of TS (**Fig. 4**). The data we present here posits a working model that accounts the molecular changes occurring postsynaptically when mTOR switches from being dynamic (**Fig. 4A**) to being persistently active (**Fig. 4B**). While an overactive mTOR state greatly impedes L-VDCC activity, boosting L-type channels can ameliorate both the molecular and physiological dysfunctions that may underlie TS-associated seizures.

Ca^{2+} channels are under-characterized in TS. Our findings that α2δ2 expression is dysregulated in TS and that it regulates GluA expression on the membrane surface, and considering its association with calcium channels argue the value of investigating the calcium channel proteome in TS and other mTORopathies (**Fig. 2**). Furthermore, as BayK does not fully suppress pS6 levels, consideration of L-VDCC activation as a therapeutic avenue should be investigated since this pathway, unlike rapamycin, may still be able to promote mTORC1-dependent syntheses of proteins that may be integral in maintaining normal synaptic function (9, 11). Current therapeutic mitigation of seizures and TS focuses on mTOR and GluA (1, 44, 47, 50-52). Their broad influence and psychiatric side effects, however, limit their clinical utility. Our collective mechanistic and functional findings downstream of mTOR offer another pathway to alleviate TS-associated neurological disorders.

Methods

Connectivity Map (CMAP) linked user environment (CLUE) analysis

To identify perturbagens that can elicit upregulation of active-mTORC1-repressed proteins, we seeded CLUE with a set of proteins whose expression levels in the PSD increase with rapamycin, as determined by Niere et al (2016) (9), and whose mRNAs contain putative DJ-1 binding sites (20, 21, 53).

Generation of TS mice

Tsc1^{tm1Djk}*/J* mice (Jackson Laboratory, Bar Harbor, ME) were used for *in vivo* and *in vitro* experiments. Recombinant adeno-associated virus coding for Cre recombinase (AAV-Cre-GFP) was introduced in *Tsc1*^{tm1Djk}*/J* mice to knockout the *Tsc1* gene and generate the TS mice. AAV-GFP (vector) was introduced to serve as control (9). A synapsin promoter was used to drive both AAV-GFP and AAV-CRE-GFP.

Primary neuronal cell culture

Embryonic rat pups (E17–18) were used to generate dissociated hippocampal neurons. Rat neuronal cultures were used for experiments at 18–25 days *in vitro* (DIV). For *Tsc1* cultures, neurons were prepared from male and female postnatal (0–3 days) *Tsc1* conditional knockout pups similar to Niere *et al* (54).

Pharmacology

(S)-(-)-Bay-K-8644 (Tocris) dissolved in DMSO (Sigma Aldrich) was used for experiments involving BayK. In **Fig. 1 to 3F**, a final concentration of 0.2-2.0 mg/kg of

BayK was injected intrapertioneally. These concentrations lower DJ-1 levels in TS mice. As 0.2 and 1.0 mg/kg BayK abates DJ-1 expression in TS, this concentration was used in **Fig. 3G to 4**. Nimodipine (Tocris), dissolved in DMSO, was used at a final concentration of 5 μM.

Transfection

Primary hippocampal neurons were transiently transfected on DIV 14 with α2δ2 (Addgene) or pcDNA plus RFP plasmid. α2δ2 HA pMT2 was a gift from Annette Dolphin (55). Hippocampal cultures were transfected with Lipofectamine 2000 (Invitrogen) according to the manufacturer's instructions. Transfection was allowed to occur for 2.5 hours. Cells were processed for immunohistochemistry on DIV18.

Immunohistochemistry (IHC)

Dissociated hippocampal neurons were fixed in 4% paraformaldehyde for 20 minutes at room temperature and permeabilized in 0.2% Triton X-100 for 10 minutes(54). Fixed cells were incubated overnight in 4°C with the following primary antibodies: rabbit anti-α2δ2 (1:500, Alomone), rabbit anti-DJ-1 (1:1000, Novus), chicken anti-Map2 (1:1000, Aves), mouse anti-Map2 (1:1000, Abcam). For detection of surface GluA1 in rat hippocampal neurons, the cells were fixed in 4% paraformaldehyde for 8 minutes on ice to prevent permeabilization. After blocking in 8% normal goat serum (NGS) for an hour at RT, the cells were incubated with a mouse anti-GluA1 N-terminal antibody (1:100, Millipore) overnight at 4°C. The cells were then washed with PBS, permeabilized for 5 minutes and incubated with either chicken or mouse anti-Map2 for 1 hr at RT. Appropriate secondary antibodies (1:500, Life Technologies) were then used. For

detection of surface GluA1 in mouse WT or Tsc1 KO neurons, the cells were incubated with a rabbit anti-GluA1 N-terminal antibody (Calbiochem) for 10 minutes at 37°C. The cells were then fixed on ice for 5 minutes and then incubated with an AlexaFluor647 for 1hr at RT to saturate surface GluA1. Permeabilization and blocking was then performed followed by incubation with chicken anti-Map2 ON at 4°C. Appropriate secondary antibodies (1:500, Life Technologies) were used—AlexaFluor488 (AF488), AF647, AF405—after overnight primary antibody incubation.

Western blots

Synaptoneurosome preparation

Hippocampi were homogenized with lysis buffer composed of Tris-Base with Halt™ Phosphatase and Protease Inhibitor Cocktail (Thermo Scientific). Homogenates were filtered through 100μm cell strainer and 5μm syringe filter, sequentially, and centrifuged for 20 minutes in 4°C at 14,000 xg. The pellet was retained, solubilized in radioimmunoprecipitation (RIPA) buffer, and centrifuged for 10 minutes in 4°C at 14,000 xg. Pierce™ BCA Protein Assay Kit (Thermo Scientific) was used to quantify protein in the collected supernatant.

Western blot analysis

SDS-polyacrylamide gel electrophoresis (PAGE) loading buffer using 4x Laemmli Sample Buffer (Bio-Rad) was added to protein samples. 20 to 50 μg protein from each sample were resolved in 10% SDS-polyacrylamide gel and transferred onto 0.2 μm nitrocellulose membranes (Bio-Rad). 5% nonfat dry milk in Tris-buffered saline containing 0.1% Tween 20 was use to block the membranes. To visualize the proteins,

we used: mouse anti-DJ1 (1:2000; Novus Biologicals), rabbit anti-phospho-GluA1 (Ser845, 1:1000, R&D Systems), mouse anti-GluA1 (1:2000, Neuromab), mouse anti-ribosomal S6 (1:1000, Cell Signaling), rabbit anti-phospho-S6 (1:1000, Cell Signaling), and mouse anti-tubulin (1:20,000; Abcam). Fluorescence-conjugated secondary antibodies (AF680, Life Technologies; AF800, LiCor; 1:5000) were used to visualize the proteins of interest. Immunoblots were obtained using the Odyssey CLx infrared imaging system. Densitometric quantification of proteins was performed using ImageJ (National Institutes of Health) software.

In vivo recording

Electrode implantation

Approximately 3-month old *Tsc1tm1Djk*/J mice were anesthetized with isoflurane and placed in a stereotaxic device. As previously described, metal ground screws were secured to the cranium bilaterally and tungsten microwires were implanted in a satellite array in cortical, subcortical, and hippocampal locations(40). AAV-Cre-GFP or AAV-GFP was introduced into the hippocampus just prior to electrode implantation.

Data acquisition and analyses

Mice were allowed to recover one week before recordings. Wideband (0.3–20 kHz, sampled at 40 kHz) depth recordings were made using the SciWorks recording system (DataWave Technologies), AM-3600 extracellular amplifiers (A-M Systems), and T8G100 headstage amplifiers (TBSI). Data analysis was performed using custom scripts written in MATLAB (MathWorks). Seizures were detected as follows: raw signals from the recording array were transformed using the Teager Energy Operator (56),

followed by calculation of the smoothed sliding window (10 ms) root-mean-square (RMS) and then z-scored using the mean and standard deviation of baseline recordings. Seizures were detected using a threshold of 10 sigma which was chosen to minimize the false negative rate. False positives were manually excluded. Experimenters were blinded to condition during analyses. Seizure duration was defined as the window between pre-and post-ictal baseline periods detected by a drop in the zscore of the sliding window RMS of the wideband signal to below 1 sigma for pre-ictal and -1 sigma for post-ictal.

Acknowledgments

We would like to thank Dr. Sanjeev Namjoshi for his helpful discussions regarding the connectivity mapping. This study was supported by National Institutes of Health NINDS NS105005 (KRG); AA016852 (DCK, TS, DWG) the National Science Foundation IOS 1355158 and 1724812 (KRG), Postdoctoral Research Fellowship in Biology DBI-1306528 (FN) and DBI-1103738 (LPC); Alzheimer's Association AARF-19-614794 (FN); Department of Defense, United States Army Medical Research and Materiel Command USAMRMC Award W81XWH-14-1-0061 and W81XWH-19-1-0202 (KRG). National Institute of Aging Wake Forest School of Medicine Alzheimer's Disease Research Center Pilot Grant P30AG049638 (KRG).

Author contributions: FN, LPC, DCK and KRG designed research. FN, LPC, DCK, WCT, and TS conducted experiments and analyzed data. FN, LPC, and KRG wrote the manuscript.

Figure Legend

Figure 1. Boosting L-type VDCC activity by Bay-K-8644 (BayK) in a mouse model of tuberous sclerosis (TS) restores excessive DJ-1 expression. **(A)** 121 or 13% of epilepsy- and ASD-risk genes are associated with the PSD and contain several putative DJ-1-binding sequences (GNGCNG and CNGCNG). **(B and C)** Western blot experiments demonstrate that 18-20 hours post-administration of BayK (0.2 to 2 mg/kg) in TS mice lowers synaptic DJ-1 to wildtype (WT) level. **(B)** Representative Western blot of DJ-1 and tubulin and their normalized densitometric values provided below each band. Values are normalized to WT. **(C)** Quantification of Western blot experiments normalized to WT (TS: 1.85±0.23, n=4; TS+BayK: 0.68±0.12, n=4; WT: 1.00±0.16, n=7; one-way ANOVA). Values are shown as mean±s.e.m.

Figure 2. BayK or overexpression of calcium channel-associated protein α2δ2 in TS neurons corrects the excessive expression of GluA on the dendritic membrane. **(A-D)** L-type calcium channels control the surface expression of GluA (sGluA). **(A-B)** Dissociated rat hippocampal neurons treated with L-type VDCC blocker nimodipine (Nimo; 5 μM) have fewer sGluA compared to control (Ctl) as shown by **(A)** representative figures and **(B)** quantification of sGluA normalized to Ctl (Ctl: 1.00±0.14, n=19; Nimo: 1.87±0.42, n=13; student's t-test). **(C-D)** Excess sGluA levels in TS can be curtailed by application of BayK (5 mM) to WT status as depicted in **(C)** representative figures and **(D)** quantification of sGluA normalized to WT (TS: 2.54±0.60, n=18; TS+BayK: 1.12±0.36, n=20; WT: 1.00±0.26, n=16; one-way ANOVA). **(E-H)** Levels of

Cacna2d2 gene, which encodes α2δ2 protein, regulate sGluA expression. **(E-F)** Overexpressing *Cacna2d2* in dissociated rat hippocampal neurons diminishes sGluA levels compared to Ctl as shown by **(E)** representative figures and **(F)** quantification of sGluA normalized to Ctl (Ctl: 1.00±0.15, n=25; *Cacna2d2*: 0.44±0.08, n=25; student's t-test). **(G-H)** Overexpression of *Cacna2d2* in TS lowers elevated sGluA to WT level as depicted in **(G)** representative figures and **(H)** quantification of sGluA normalized to WT (TS: 3.48±0.62, n=14; TS+*Cacna2d2*: 1.63±0.26, n=19; WT: 1.00±0.19, n=12; one-way ANOVA). Map2 indicates dendrites. Values are shown as mean±s.e.m.

Figure 3. Peripheral administration of BayK in TS mitigates key components of seizure neuropathophysiology. **(A-C)** Acute intraperitoneal (i.p.) injection of BayK (0.2-2 mg/kg) lowers synaptic GluA in TS mice to WT status. **(A)** Representative Western blot of GluA1 phosphorylated at serine 845 (pGluA1), total GluA1 and tubulin and their normalized densitometric values indicated below each band. Values are normalized to WT. **(B)** Quantification of pGluA1 (TS: 1.35±0.43, n=4; TS+BayK: 0.87±0.38, n=5; WT: 1.00±0.18, n=7; one-way ANOVA). **(C)** Quantification of GluA1 (TS: 1.89±0.43; TS+BayK: 0.99±0.45; WT: 1.00±0.19). **(D-F)** Acute i.p. injection of BayK (0.2-2 mg/kg) lowers synaptic ribosomal S6 (S6) protein in TS to WT status. **(D)** Representative Western blot of phosphorylated S6 (pS6), total S6 and tubulin and their normalized densitometric values indicated below each band. Values are normalized to WT. **(E)** Quantification of pS6 (TS: 6.04±1.32, n=4; TS+BayK: 3.34±0.93, n=5; WT: 1.00±0.02, n=7; one-way ANOVA). **(F)** Quantification of S6 (TS: 2.79±0.59; TS+BayK: 1.24±0.30; WT: 1.00±0.12). **(G-H)** Acute and chronic administration of BayK (0.2-1.0 mg/kg) in TS

abates frequency and duration of seizures. **(G)** Representative electrophysiological seizures in TS. **(H)**. Quantification of seizure frequency (TS+Veh: 10±2, n=6; TS+BayK: 2±1, n=5; student's t-test). **(I)** Quantification of seizure duration (TS+Veh: 365±127, n=6; TS+BayK: 51±36, n=5). Values are shown as mean±s.e.m.

Figure 4. Administering BayK to TS extends life expectancy. **(A-B)** Acute i.p. injection of BayK (0.2-1 mg/kg) lengthens TS lifespan. **(A)** TS have shorter lifespan than GFP/control mice (GFP/green: undefined (>70), TS/red: 40). Values are median survival days. Significance is determined by log-rank test. **(B)** Chronically implanted/recorded and non-implanted TS mice receiving BayK live longer than their respective vehicle (Veh) counterparts. Values normalized to Veh (Veh: 1.00±0.07, n=7; BayK: 1.27±0.15, n=6; student's t-test). Values are shown as mean±s.e.m. **(C)**. Working model underlying L-VDCC-mediated neuropathophysiology in TS. **(C1)** Under normal conditions, the dynamic state of mTOR activity allows DJ-1-regulated events (L-VDCC activity and α2δ2 expression) in dendrites to respond to synaptic stimuli accordingly. L-VDCC activity modulates GluA expression on the dendritic membrane. α2δ2 influences the stability and trafficking of L-VDCC to the membrane surface. **(C2)** In a persistent active mTOR state, elevated DJ-1 represses L-VDCC activity and diminishes α2δ2 level. Weakened L-VDCC activity, either through DJ-1/L-VDCC or DJ-1/ α2δ2 interaction or both, promotes more expression of GluA on the membrane. Consequently, overabundance of GluA favors the generation of seizures that can lower life expectancy. **(C3)** Boosting L-VDCC activity by BayK in a persistently active mTOR state (e.g. TS) diminishes the frequency and duration of seizures and extends life expectancy

potentially through 3 mechanisms: (1) lowering DJ-1 levels (i.e. reversing the effects of excess DJ-1; *see Fig. 1B-C*), (2) decreasing surface expression of GluA (*see Fig. 2B-C*), and (3) reducing mTOR activity (*see Fig. 3D-F*).

Reference

1. Davis PE, Peters JM, Krueger DA, & Sahin M (2015) Tuberous Sclerosis: A New Frontier in Targeted Treatment of Autism. *Neurotherapeutics* 12(3):572-583.
2. Leclezio L & de Vries PJ (2015) Advances in the treatment of tuberous sclerosis complex. *Current opinion in psychiatry* 28(2):113-120.
3. Kanner AM (2016) Management of psychiatric and neurological comorbidities in epilepsy. *Nature reviews. Neurology* 12(2):106-116.
4. Sahin M*, et al.* (2016) Advances and Future Directions for Tuberous Sclerosis Complex Research: Recommendations From the 2015 Strategic Planning Conference. *Pediatric neurology* 60:1-12.
5. Raab-Graham KF & Niere F (2017) mTOR referees memory and disease through mRNA repression and competition. *FEBS letters* 591(11):1540-1554.
6. Tang SJ*, et al.* (2002) A rapamycin-sensitive signaling pathway contributes to long-term synaptic plasticity in the hippocampus. *Proc Natl Acad Sci U S A* 99(1):467-472.
7. Raab-Graham KF, Haddick PC, Jan YN, & Jan LY (2006) Activity- and mTOR-dependent suppression of Kv1.1 channel mRNA translation in dendrites. *Science* 314(5796):144-148.
8. Auerbach BD, Osterweil EK, & Bear MF (2011) Mutations causing syndromic autism define an axis of synaptic pathophysiology. *Nature* 480(7375):63-68.
9. Niere F*, et al.* (2016) Analysis of Proteins That Rapidly Change Upon Mechanistic/Mammalian Target of Rapamycin Complex 1 (mTORC1) Repression Identifies Parkinson Protein 7 (PARK7) as a Novel Protein Aberrantly Expressed in Tuberous Sclerosis Complex (TSC). *Mol Cell Proteomics* 15(2):426-444.
10. Saxton RA & Sabatini DM (2017) mTOR Signaling in Growth, Metabolism, and Disease. *Cell* 168(6):960-976.
11. Niere F & Raab-Graham KF (2017) mTORC1 Is a Local, Postsynaptic Voltage Sensor Regulated by Positive and Negative Feedback Pathways. *Front Cell Neurosci* 11:152.
12. Henry FE*, et al.* (2018) A Unique Homeostatic Signaling Pathway Links Synaptic Inactivity to Postsynaptic mTORC1. *J Neurosci* 38(9):2207-2225.
13. McCabe MP*, et al.* (2020) Genetic inactivation of mTORC1 or mTORC2 in neurons reveals distinct functions in glutamatergic synaptic transmission. *eLife* 9.
14. Kimbrell TA*, et al.* (1999) Frequency dependence of antidepressant response to left prefrontal repetitive transcranial magnetic stimulation (rTMS) as a function of baseline cerebral glucose metabolism. *Biological psychiatry* 46(12):1603-1613.
15. Speer AM*, et al.* (2000) Opposite effects of high and low frequency rTMS on regional brain activity in depressed patients. *Biological psychiatry* 48(12):1133-1141.
16. Ressler KJ & Mayberg HS (2007) Targeting abnormal neural circuits in mood and anxiety disorders: from the laboratory to the clinic. *Nat Neurosci* 10(9):1116-1124.
17. Gunn BG & Baram TZ (2017) Stress and Seizures: Space, Time and Hippocampal Circuits. *Trends Neurosci* 40(11):667-679.

18. Sosanya NM*, et al.* (2013) Degradation of high affinity HuD targets releases Kv1.1 mRNA from miR-129 repression by mTORC1. *J Cell Biol* 202(1):53-69.
19. Keene JD (2007) RNA regulons: coordination of post-transcriptional events. *Nature reviews. Genetics* 8(7):533-543.
20. Lamb J*, et al.* (2006) The Connectivity Map: using gene-expression signatures to connect small molecules, genes, and disease. *Science* 313(5795):1929-1935.
21. Subramanian A*, et al.* (2017) A Next Generation Connectivity Map: L1000 Platform and the First 1,000,000 Profiles. *Cell* 171(6):1437-1452 e1417.
22. Mullins C, Fishell G, & Tsien RW (2016) Unifying Views of Autism Spectrum Disorders: A Consideration of Autoregulatory Feedback Loops. *Neuron* 89(6):1131-1156.
23. Lin JW*, et al.* (2000) Distinct molecular mechanisms and divergent endocytotic pathways of AMPA receptor internalization. *Nat Neurosci* 3(12):1282-1290.
24. Talos DM, Kwiatkowski DJ, Cordero K, Black PM, & Jensen FE (2008) Cell-specific alterations of glutamate receptor expression in tuberous sclerosis complex cortical tubers. *Ann Neurol* 63(4):454-465.
25. Tavazoie SF, Alvarez VA, Ridenour DA, Kwiatkowski DJ, & Sabatini BL (2005) Regulation of neuronal morphology and function by the tumor suppressors Tsc1 and Tsc2. *Nat Neurosci* 8(12):1727-1734.
26. Bateup HS, Takasaki KT, Saulnier JL, Denefrio CL, & Sabatini BL (2011) Loss of Tsc1 in vivo impairs hippocampal mGluR-LTD and increases excitatory synaptic function. *J Neurosci* 31(24):8862-8869.
27. Lissin DV*, et al.* (1998) Activity differentially regulates the surface expression of synaptic AMPA and NMDA glutamate receptors. *Proc Natl Acad Sci U S A* 95(12):7097-7102.
28. Snyder EM*, et al.* (2001) Internalization of ionotropic glutamate receptors in response to mGluR activation. *Nat Neurosci* 4(11):1079-1085.
29. Xiao MY, Zhou Q, & Nicoll RA (2001) Metabotropic glutamate receptor activation causes a rapid redistribution of AMPA receptors. *Neuropharmacology* 41(6):664-671.
30. Dolphin AC (2012) Calcium channel auxiliary alpha2delta and beta subunits: trafficking and one step beyond. *Nat Rev Neurosci* 13(8):542-555.
31. Dolphin AC (2013) The alpha2delta subunits of voltage-gated calcium channels. *Biochim Biophys Acta* 1828(7):1541-1549.
32. Dolphin AC (2016) Voltage-gated calcium channels and their auxiliary subunits: physiology and pathophysiology and pharmacology. *J Physiol* 594(19):5369-5390.
33. Lee HK, Barbarosie M, Kameyama K, Bear MF, & Huganir RL (2000) Regulation of distinct AMPA receptor phosphorylation sites during bidirectional synaptic plasticity. *Nature* 405(6789):955-959.
34. Schratt GM, Nigh EA, Chen WG, Hu L, & Greenberg ME (2004) BDNF regulates the translation of a select group of mRNAs by a mammalian target of rapamycin-phosphatidylinositol 3-kinase-dependent pathway during neuronal development. *J Neurosci* 24(33):7366-7377.
35. Slipczuk L*, et al.* (2009) BDNF activates mTOR to regulate GluR1 expression required for memory formation. *PLoS One* 4(6):e6007.

36. Chu-Shore CJ, Major P, Camposano S, Muzykewicz D, & Thiele EA (2010) The natural history of epilepsy in tuberous sclerosis complex. *Epilepsia* 51(7):1236-1241.
37. Vignoli A*, et al.* (2013) Epilepsy in TSC: certain etiology does not mean certain prognosis. *Epilepsia* 54(12):2134-2142.
38. Curatolo P, Moavero R, & de Vries PJ (2015) Neurological and neuropsychiatric aspects of tuberous sclerosis complex. *Lancet Neurol* 14(7):733-745.
39. Loddenkemper T*, et al.* (2014) Subunit composition of glutamate and gamma-aminobutyric acid receptors in status epilepticus. *Epilepsy research* 108(4):605-615.
40. Klorig DC, Alberto GE, Smith T, & Godwin DW (2019) Optogenetically-Induced Population Discharge Threshold as a Sensitive Measure of Network Excitability. *eNeuro* 6(6).
41. Shepherd CW, Gomez MR, Lie JT, & Crowson CS (1991) Causes of death in patients with tuberous sclerosis. *Mayo Clinic proceedings* 66(8):792-796.
42. Webb DW, Fryer AE, & Osborne JP (1996) Morbidity associated with tuberous sclerosis: a population study. *Developmental medicine and child neurology* 38(2):146-155.
43. Moavero R, Romagnoli G, Graziola F, & Curatolo P (2015) Mammalian Target of Rapamycin Inhibitors and Life-Threatening Conditions in Tuberous Sclerosis Complex. *Seminars in pediatric neurology* 22(4):282-294.
44. Curatolo P, Jozwiak S, Nabbout R, SEGA TSCCMf, & Epilepsy M (2012) Management of epilepsy associated with tuberous sclerosis complex (TSC): clinical recommendations. *European journal of paediatric neurology : EJPN : official journal of the European Paediatric Neurology Society* 16(6):582-586.
45. Meikle L*, et al.* (2007) A mouse model of tuberous sclerosis: neuronal loss of Tsc1 causes dysplastic and ectopic neurons, reduced myelination, seizure activity, and limited survival. *J Neurosci* 27(21):5546-5558.
46. Crino PB (2008) Do we have a cure for tuberous sclerosis complex? *Epilepsy Curr* 8(6):159-162.
47. Tsai P & Sahin M (2011) Mechanisms of neurocognitive dysfunction and therapeutic considerations in tuberous sclerosis complex. *Current opinion in neurology* 24(2):106-113.
48. Vignoli A*, et al.* (2015) Autism spectrum disorder in tuberous sclerosis complex: searching for risk markers. *Orphanet journal of rare diseases* 10:154.
49. Kabir ZD, Martinez-Rivera A, & Rajadhyaksha AM (2017) From Gene to Behavior: L-Type Calcium Channel Mechanisms Underlying Neuropsychiatric Symptoms. *Neurotherapeutics* 14(3):588-613.
50. Ostendorf AP & Wong M (2015) mTOR inhibition in epilepsy: rationale and clinical perspectives. *CNS drugs* 29(2):91-99.
51. Sadowski K, Kotulska-Jozwiak K, & Jozwiak S (2015) Role of mTOR inhibitors in epilepsy treatment. *Pharmacological reports : PR* 67(3):636-646.
52. McEneaney LJ & Tee AR (2019) Finding a cure for tuberous sclerosis complex: From genetics through to targeted drug therapies. *Advances in genetics* 103:91-118.

53. Lamb J (2007) The Connectivity Map: a new tool for biomedical research. *Nature reviews. Cancer* 7(1):54-60.
54. Niere F, Wilkerson JR, & Huber KM (2012) Evidence for a fragile X mental retardation protein-mediated translational switch in metabotropic glutamate receptor-triggered Arc translation and long-term depression. *J Neurosci* 32(17):5924-5936.
55. Davies A*, et al.* (2006) The calcium channel alpha2delta-2 subunit partitions with CaV2.1 into lipid rafts in cerebellum: implications for localization and function. *J Neurosci* 26(34):8748-8757.
56. Boudraa AO & Salzenstein F (2018) Teager–Kaiser energy methods for signal and image analysis: A review. *Digit Signal Process* 78:37.

Figure 1

A

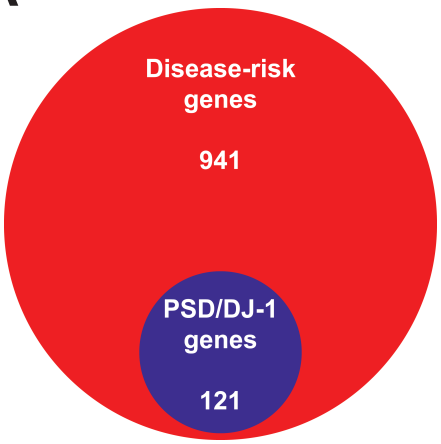
Disease-risk genes
941
PSD/DJ-1 genes
121

B

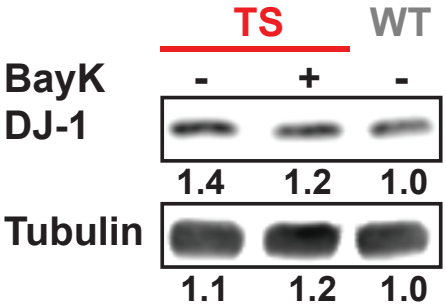
TS
WT
BayK
-
+
-
DJ-1
1.4
1.2
1.0
Tubulin
1.1
1.2
1.0

C

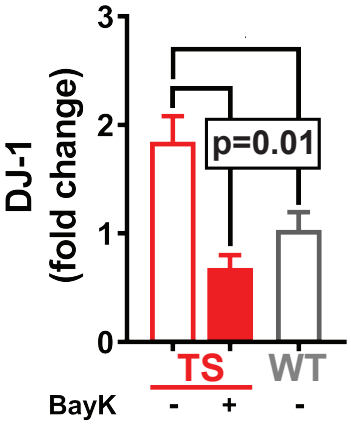
DJ-1 (fold change)
3
2
1
0
p=0.01
TS
WT
BayK
-
+
-

Figure 2

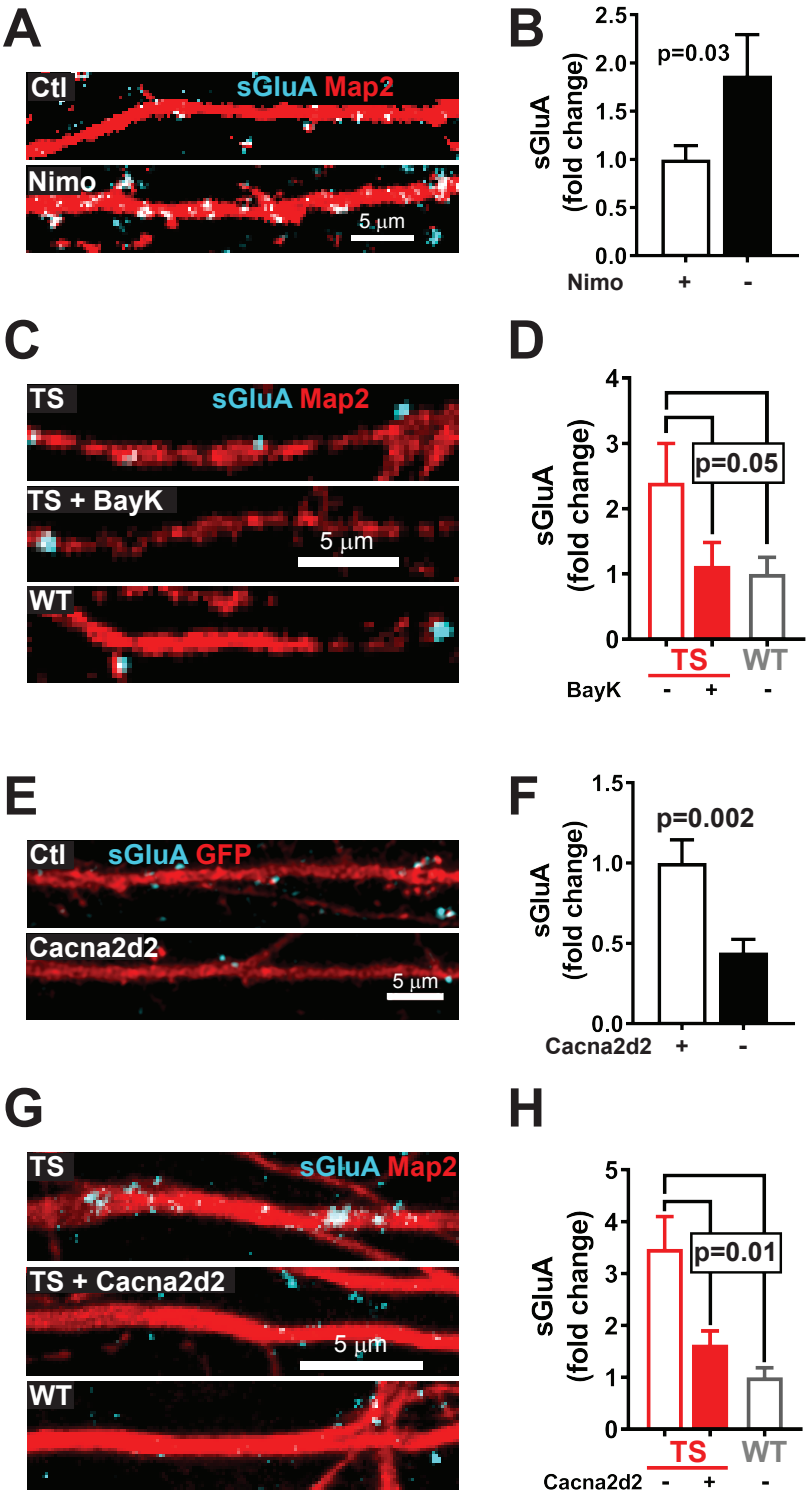
A
Ctl
sGluA Map2
Nimo
5 µm
B
sGluA (fold change)
p=0.03
Nimo
+
-
C
TS
sGluA Map2
TS + BayK
5 µm
WT
D
sGluA (fold change)
p=0.05
TS
WT
BayK
-
+
-
E
Ctl
sGluA GFP
Cacna2d2
5 µm
F
sGluA (fold change)
p=0.002
Cacna2d2
+
-
G
TS
sGluA Map2
TS + Cacna2d2
5 µm
WT
H
sGluA (fold change)
p=0.01
TS
WT
Cacna2d2
-
+
-

Figure 3

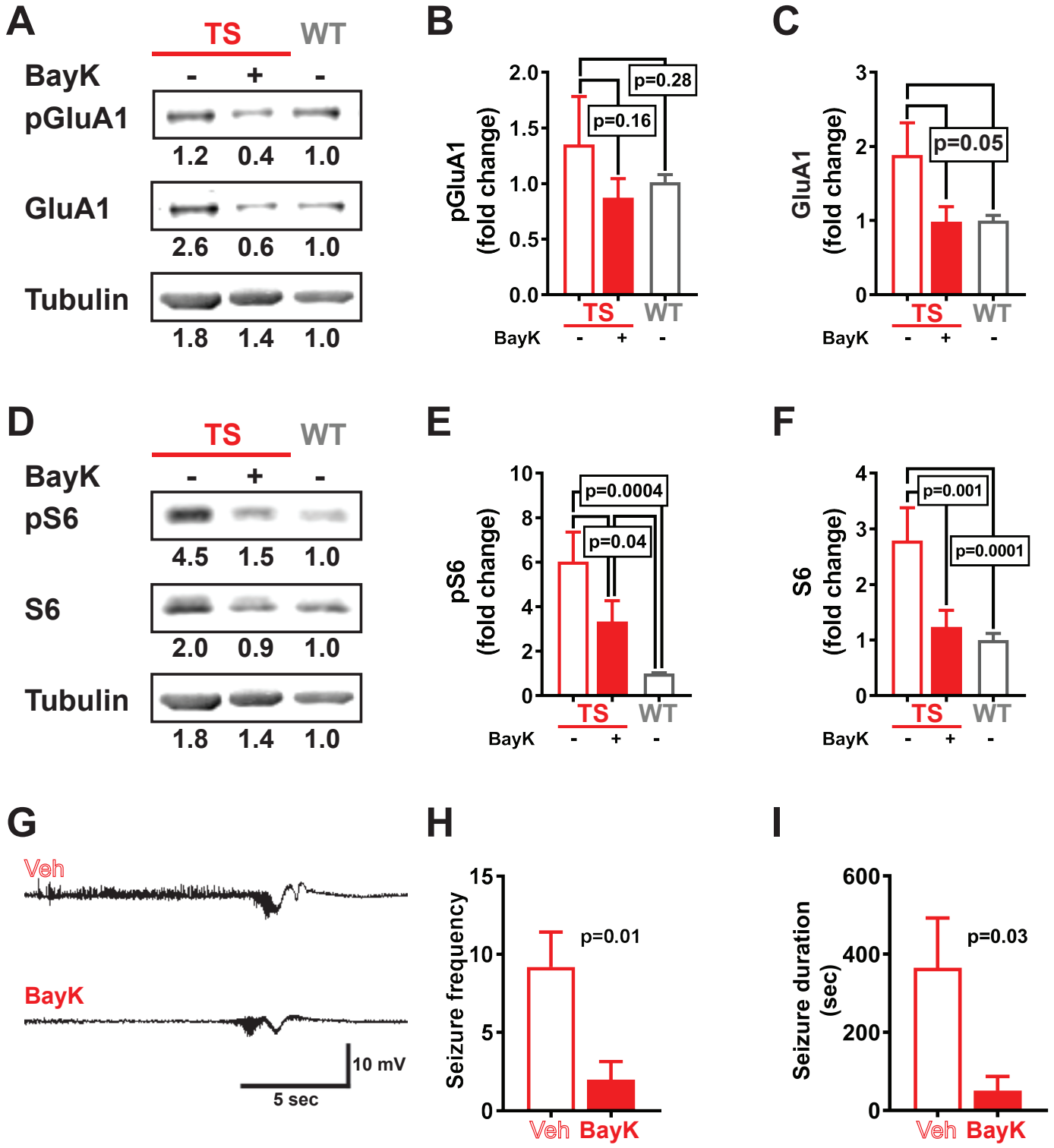
A
TS
WT
BayK
- + -
pGluA1
1.2 0.4 1.0
GluA1
2.6 0.6 1.0
Tubulin
1.8 1.4 1.0
B
pGluA1 (fold change)
2.0
1.5
1.0
0.5
0.0
p=0.28
p=0.16
TS
WT
BayK - + -
C
GluA1 (fold change)
3
2
1
0
p=0.05
TS
WT
BayK - + -
D
TS
WT
BayK
- + -
pS6
4.5 1.5 1.0
S6
2.0 0.9 1.0
Tubulin
1.8 1.4 1.0
E
pS6 (fold change)
10
8
6
4
2
0
p=0.0004
p=0.04
TS
WT
BayK - + -
F
S6 (fold change)
4
3
2
1
0
p=0.001
p=0.0001
TS
WT
BayK - + -
G
Veh
BayK
10 mV
5 sec
H
Seizure frequency
15
10
5
0
p=0.01
Veh
BayK
I
Seizure duration (sec)
600
400
200
0
p=0.03
Veh
BayK

Figure 4

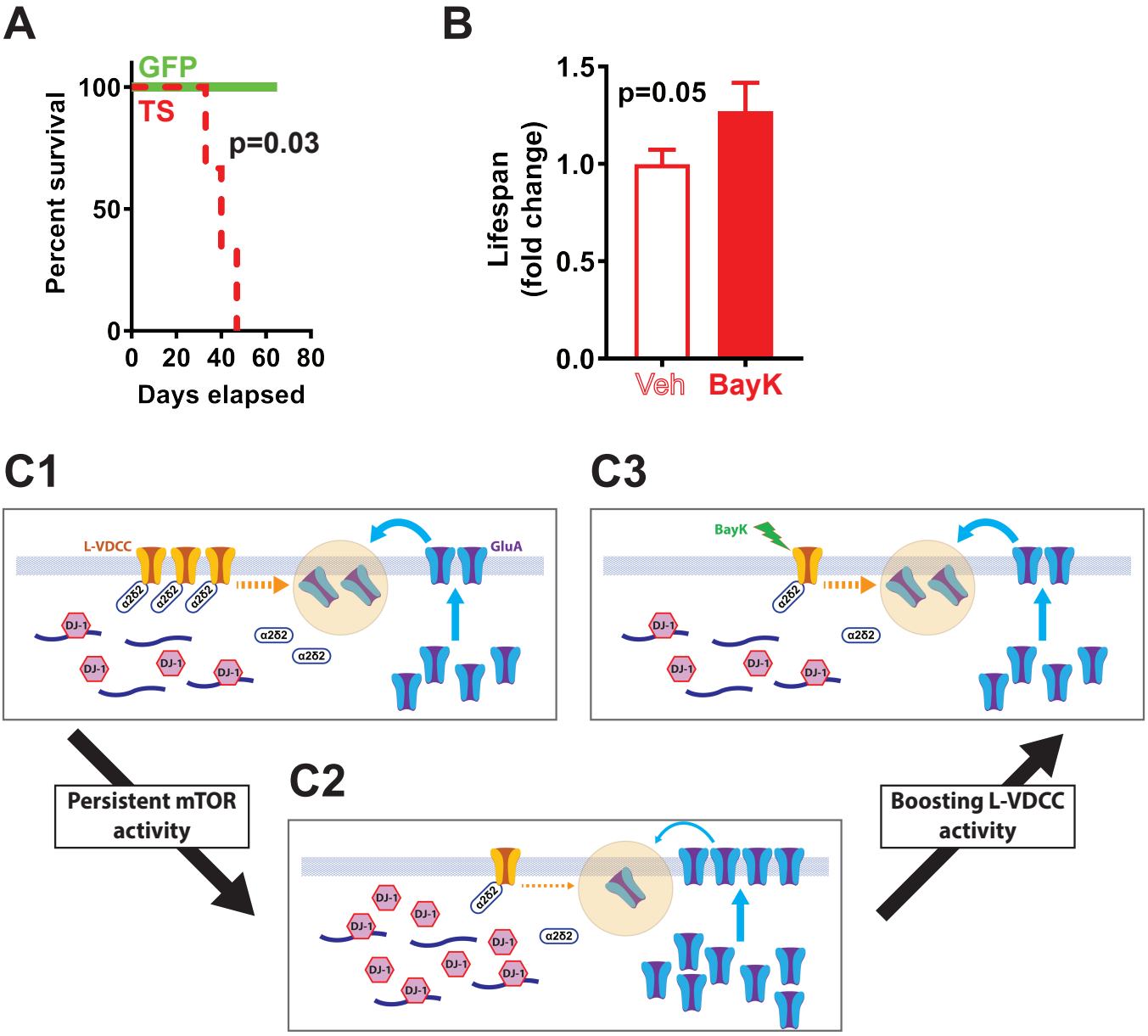
A
GFP
TS
p=0.03
Percent survival
100
50
0
0 20 40 60 80
Days elapsed
B
p=0.05
Lifespan
(fold change)
1.5
1.0
0.5
0.0
Veh
BayK
C1
L-VDCC
GluA
α2δ2
DJ-1
C2
C3
BayK
Persistent mTOR activity
Boosting L-VDCC activity